Magnetization and Mössbauer study of the reentrant amorphous $Fe_{90}Zr_{10}$ alloy

S. N. Kaul and V. Siruguri
School of Physics, University of Hyderabad, Hyderabad 500134, Andhra Pradesh, India

G. Chandra
Low Temperature Physics Group, Tata Institute of Fundamental Research, Bombay 400 005, India
(Received 4 September 1991; revised manuscript received 17 January 1992)

A detailed analysis of the magnetization and "zero-field" Mössbauer data taken on the amorphous $Fe_{90}Zr_{10}$ alloy in the temperature range 4.2–300 K reveals the following: (i) Spin-wave (SW) excitations at low temperatures, single-particle (SP) excitations and *local*-spin-density (LSD) fluctuations over a wide range of intermediate temperatures, and enhanced fluctuations in the *local* magnetization for temperatures close to the Curie temperature, T_C, contribute dominantly to the thermal demagnetization of spontaneous magnetization; (ii) SW modes soften at temperatures below the freezing temperature T_f, where long-range ferromagnetic order coexists with the cluster spin-glass order; (iii) the LSD fluctuations are completely suppressed when magnetic fields (H) higher than 5 kOe are applied and $M(H,T)$ for $H > 5$ kOe is solely governed by the SW and SP excitations for temperatures up to $0.95T_C$; (iv) contrary to some earlier claims, the spin-wave stiffness coefficient does not depend on H in the field range 5 kOe $\leq H \leq$ 15 kOe; (v) the magnetic hyperfine-field distribution, $P(H_{hf})$, is *bimodal* and comprises two Gaussian distributions; (vi) the low-field spin fraction [ratio of the area under the low-field Gaussian curve to that under the $P(H_{hf})$-vs-H_{hf} curve] grows at the expense of the high-field spin fraction as the temperature is raised above $T \simeq 150$ K and amounts to about 90% of the total Fe spins for $T \simeq T_C$; and (vii) the spin-freezing process does not start abruptly at T_f but proceeds gradually over a wide temperature range extending from 130 K ($\approx 3T_f$) down to 4.2 K. While the transverse spin freezing and the finite spin clusters (composed of antiferromagnetic Fe spins) plus ferromagnetic (FM) matrix models fail to explain some of our findings, the finite-FM-clusters–FM-matrix picture provides a satisfactory explanation for all the diverse aspects of the present results.

I. INTRODUCTION

The phenomenon of reentrance, i.e., the transition from paramagnetic (PW) to ferromagnetic (FM) state at a critical temperature T_C (Curie point) is followed at a lower temperature T_f by another transition from FM to a "spin-glass-like" (reentrant) state, usually exhibited by both crystalline and amorphous magnetic systems in which the concentration of the moment bearing atoms just exceeds the percolation threshold, has received considerable scientific attention particularly during the latter half of the past decade. Amorphous (a-) $Fe_{100-x}Zr_x$ alloys with x near 10 at. %, owing to their unusually complex magnetic behavior, rank among the most extensively studied amorphous spin systems. As a result of intense experimental efforts which involve magnetization,[1–5] Mössbauer,[6–16] ac susceptibility,[17–21] ferromagnetic resonance,[22–25] pulsed nuclear magnetic resonance,[26] Lorentz transmission electron microscopy,[27,28] small-angle neutron scattering[29] (SANS), electric resistivity,[30–32] magnetoresistivity,[33] and thermoelectric power[34] measurements on Fe-rich a-$Fe_{100-x}Zr_x$ alloys, a transition to the state with long-range ferrromagnetic ordering at T_C is now relatively well established, but the exact nature of the transition at T_f and that of the reentrant state has eluded a clear-cut understanding so far. The changes in various *characteristic* physical parameters, consequent upon a transition to the reentrant state, have been basically understood from *three divergent* points of view. The first approach[9,10,12,13,16] considers the reentrant phase as a mixed phase[35] in which ferromagnetic order along the z direction coexists with spin-glass order in the xy directions. The second school of thought[1,18,20] regards the reentrant state as consisting of the *spin clusters* of *antiferromagnetic* (AFM) Fe spins and the *ferromagnetic* Fe-Zr *matrix* in which these clusters are frozen in random orientations. According to the third model,[4,5,11,15,19,22,24,36] the spin system for $T \lesssim T_f$ comprises the *infinite* three-dimensional (3D) ferromagnetic network (matrix) and the *finite* spin clusters (composed of a set of ferromagnetically coupled spins) which are frozen in random directions and embedded in the FM matrix. Although all three models concur in that the reentrant state is a mixed state, the underlying mechanism varies from model to model. For instance, the longitudinal and transverse spin components coexist at every site and hence the spin system is perfectly *homogeneous* even on the microscopic scale in the transverse spin-freezing model,[35] as contrasted with the spatial segregation of finite spin clusters and FM matrix in the other two models. The spatial segregation of the type just mentioned arises from the *concentration fluctuations*[18] [i.e., the glassy alloys in question consist of Fe-rich regions in which a given Fe atom has only Fe neighbors in a fcc-like

nearest-neighbor coordination (AFM Fe clusters), and the remaining Fe-poor bulk (FM matrix), in which a given Fe atom has at least one Zr neighbor] in the AFM clusters plus FM matrix picture,[1,18] whereas it originates from the *density fluctuations*[5] [i.e., in a-$Fe_{90\pm x}Zr_{10\mp x}$ alloys, which are homogeneous so far as the chemical composition is concerned, microscopic regions of low-density exist in an otherwise high-density bulk such that the average nearest-neighbor (NN) distance between Fe atoms in these "low-density pockets" is appreciably *greater* than that in the remaining bulk, and as a consequence the ferromagnetic coupling between spins within the finite clusters (low-density regions) is much stronger than that between the spins in the FM matrix (high-density bulk); for details see Ref. 5] in the finite-FM-spin-clusters–3D-FM-matrix model.

A detailed magnetization (bulk) and "zero-field" Mössbauer (local) study of the amorphous $Fe_{90}Zr_{10}$ alloy has been undertaken with a view to ascertain which of the above-mentioned models form an adequate description of the transition at T_f and the reentrant state in this material. The zero-field ^{57}Fe Mössbauer technique was particularly chosen for this type of investigation for the following reasons. First, a zero-field study is called for in view of the claim[9,10,12] that Fe-rich a-$Fe_{100-x}Zr_x$ alloys behave as a "wandering-axis ferromagnet" in which no spontaneous moment exists and even a very small external magnetic field (H) suffices to produce substantial magnetization through the alignment of the *local* FM axes. Second, the Mössbauer spectra recorded at $H=0$ not only yield the magnetic hyperfine field, which is an *intrinsic local* property of the moments within a magnetic domain and hence does not depend on the details of the domain structure, but also are free from the demagnetizing (since $H=0$) and domain-wall pinning effects. Third, the average hyperfine field $\bar{H}_{hf}$ is directly proportional to the thermal average of the component of the iron moment along the local quantization axis and as such the temperature-induced changes in the local magnetization manifest themselves in the observed temperature dependence of $\bar{H}_{hf}$.

II. EXPERIMENTAL DETAILS

Amorphous (a-) $Fe_{90}Zr_{10}$ ribbons of cross section $\approx 1.5\times 0.03$ mm^2 were prepared by the single-roller melt-quenching technique in helium atmosphere. The amorphous nature of the fabricated ribbons was confirmed by the x-ray-diffraction and high-resolution electron-microscopic methods. The "as-quenched" alloy ribbons that did not show any crystalline regions upon electron-microscopic examination were used for magnetization and Mössbauer measurements. Magnetization (M) was measured (i) as a function of temperature (T) to a relative accuracy of better than 10 ppm in the temperature range 4.2–300 K at various fixed values of H in the interval 10 Oe $\leq H \leq$ 15 kOe while the sample was either cooled from 300 to 4.2 K in a field of specified strength or first cooled down to 4.2 K in zero field and then heated from 4.2 to 300 K in a constant field of given intensity at a typical rate of $\simeq$0.5 K/min, and (ii) as a function of H in fields up to 15 kOe at nearly 5-K intervals from 4.2 to 300 K during the *heating cycle* after the sample was cooled to 4.2 K in zero field. The sample temperature (T_s), measured by precalibrated carbon-glass and Pt sensors for $T<50K$ and $T\gtrsim 50$ K, respectively, was held constant to within $\pm$50 mK at a given temperature setting in the latter case. In order to minimize the demagnetizing effects, magnetization measurements were carried out with H applied along the length within the ribbon plane.

Zero-field Mössbauer spectra were obtained in the transmission geometry at different but fixed (to within $\pm$0.1 K) absorber temperatures within the range 5 K $\leq T \leq$ 300 K using a conventional constant-acceleration spectrometer and a room-temperature 40-mCi ^{57}Co*Rh* source having an intrinsic linewidth (full width at half maximum, FWHM) of 0.235$\pm$0.005 mm s^{-1}. Typically, 10^5 counts were accumulated in each channel. Detailed account of the results, obtained from the magnetization and Mössbauer measurements performed on the same sample of the a-$Fe_{90}Zr_{10}$ alloy, and their analysis given in this paper follows the brief mention of some of the findings, based on a preliminary zero-field Mössbauer investigation, made in our earlier reports.[15]

III. RESULTS, DATA ANALYSIS, AND DISCUSSION

A. Magnetization

1. Thermomagnetic and thermoremanent effects

Thermomagnetic curves taken at various representative but constant values of H in the low-field region (10 Oe $\leq H \leq$ 100 Oe) on a-$Fe_{90}Zr_{10}$ are depicted in Fig. 1. In this figure, the continuous and dashed curves represent the data obtained when magnetization (M) at the specified field value is measured as a function of temperature while heating the sample from 4.2 K after it had been cooled to 4.2 K in *zero* field from 300 K (ZFC), and while cooling the specimen from 300 K (FC), respectively. The most striking features of these curves are a sharp increase in $M(T)$ at $T_C \cong 240$ K followed by a "demagnetization-limited-like" behavior at lower temperatures particularly for $H \lesssim 10$ Oe signaling the onset of long-range FM order and a bifurcation of the $M_{ZFC}(T)$ and $M_{FC}(T)$ curves at a temperature $T_f(H)$ which lies well below T_C and decreases roughly linearly with H. This linear dependence on H (dash-dotted straight line in Fig. 1) when extrapolated to $H=0$ gives $T_f(H=0)=40\pm 1$ K. For fields $H>500$ Oe, the bifurcation in the magnetization curves disappears completely and a normal ferromagnetic behavior persists down to 4.2 K. In addition, a steep increase in coercivity as the temperature is lowered towards 4.2 K from T_f and the thermoremanent and isothermal remanent magnetization effects have been observed at temperatures well below T_f. Observations similar to those mentioned above have previously been reported[1–3,8,9,18,19,37] for a-$Fe_{100-x}Zr_x$ alloys with $x\approx 10$ at. %. However, no general consensus as regards the interpretation of these results has emerged so

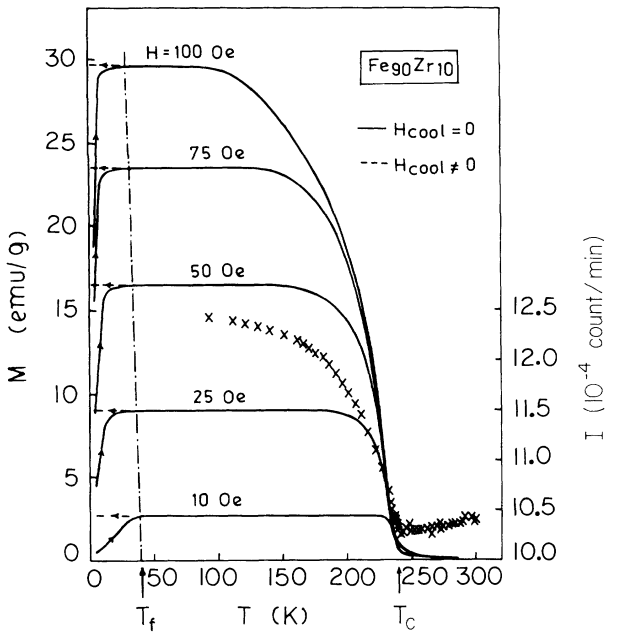

FIG. 1. Zero-velocity Mössbauer absorption (crosses) and magnetization at various constant applied field values as functions of temperature. Continuous and dashed curves depict the temperature dependence of the zero-field-cooled and field-cooled magnetization, respectively. The arrows indicate the Curie temperature T_C and the temperature T_f.

far, as is evident from the following remarks. While Read, Moyo, and Hallam[38,39] and Beck and Kronmüller[3] argue that a steep fall in $M_{ZFC}(T)$ for $T < T_f$ and the onset of irreversibility in the low-field magnetization at T_f, far from signaling a transition to a spin-glass-like state, are merely a result of failing to correct for self-demagnetization effects in the presence of exponentially increasing coercivity (caused by the pinning of domain walls by the frozen AFM spin clusters in the FM matrix) and the concomitant magnetic hardness on cooling through T_f, Ryan *et al.*[9,10] contend that H_c cannot be the cause of irreversibility as H_c is negligible at $T_f(H=0)\equiv T_{xy}$, the temperature at which the irreversible magnetization appears and the transverse (xy) components of the *local* magnetization at different sites begin to freeze in random directions in the xy plane. Within the framework of the transverse spin-freezing (TSF) model,[9,10,12,13,16] Ryan *et al.*[9,10,12] therefore propose that the thermomagnetic and thermoremanent effects in *a*-$Fe_{90\pm x}Zr_{10\mp x}$ alloys should be regarded as the characteristic properties of the spin-glass order in the xy plane. Recognizing the fact that none of these explanations can be straight away supported or rejected purely on the basis of the results obtained from the low-field magnetization measurements, and that an interpretation for the above findings similar to that given by Read, Moyo, and Hallam[38,39] can, in principle, be offered[5] in terms of the FM-spin-clusters–plus–FM-matrix picture[4,5,11,15,19,22–24,36] also, any attempt to bring about a reconciliation between different interpretations at this stage is bound to prove counterproductive.

2. *Spin-wave excitations, Stoner excitations, and local-spin-density fluctuations*

The relative deviation of "in-field" magnetization from its value at 0 K (no distinction between the values of M at 4.2 and 0 K is made in this work), i.e., $[M(H,0)-M(H,T)]/M(H,0)\equiv\Delta m$, is plotted against temperature for a few representative values of H in the range 5 kOe $\leq H \leq$ 15 kOe in Fig. 2. Recognizing the fact that the thermomagnetic and thermoremanent effects as well as the fluctuations in the *local* spin density are completely suppressed[1,2,5,37,40] in the presence of such intense fields, and that both spin-wave and single-particle excitations are expected[2,5,41] to dominantly contribute to $\Delta m(T)$, the $\Delta m(T)$ data taken at different but constant field values are analyzed in terms of the expression

$$\Delta m(T)=\Delta m_{SW}(T)+\Delta m_{SP}(T)\ , \tag{1}$$

where the spin-wave Δm_{SW} and single-particle Δm_{SP} contributions to Δm are given by[42,43]

$$\Delta m_{SW}(T)=\frac{g\mu_B}{M(H,0)}\left[Z(\tfrac{3}{2},t_H)\left[\frac{k_BT}{4\pi D(T)}\right]^{3/2}+15\pi\beta Z(\tfrac{5}{2},t_H)\left[\frac{k_BT}{4\pi D(T)}\right]^{5/2}\right] \tag{2}$$

and

$$\Delta m_{SP}(T)=\begin{cases}S(H)T^{3/2}\exp(-\Delta/k_BT)\ , & \text{for } \textit{strong} \text{ itinerant ferromagnet} \quad (3a)\\ S(H)T^2\ , & \text{for } \textit{weak} \text{ itinerant ferromagnet}\ . \quad (3b)\end{cases}$$

In Eq. (2), the Bose-Einstein integral functions

$$Z(s,t_H)=\sum_{n=1}^{\infty} n^{-s}\exp(-nt_H) \tag{4}$$

with

$$t_H=T_g/T=g\mu_BH_{eff}/k_BT \tag{5}$$

allow for the extra energy gap, $g\mu_BH_{eff}$ ($=k_BT_g$), in the spin-wave spectrum arising from the effective field

$$H_{eff}=H-4\pi NM+H_A\ , \tag{6}$$

(where N, M, and H_A are the demagnetizing factor, spontaneous magnetization, and anisotropy field, respectively) which the spins experience within the sample, and the spin-wave stiffness coefficient D renormalizes with temperature according to the relations[5]

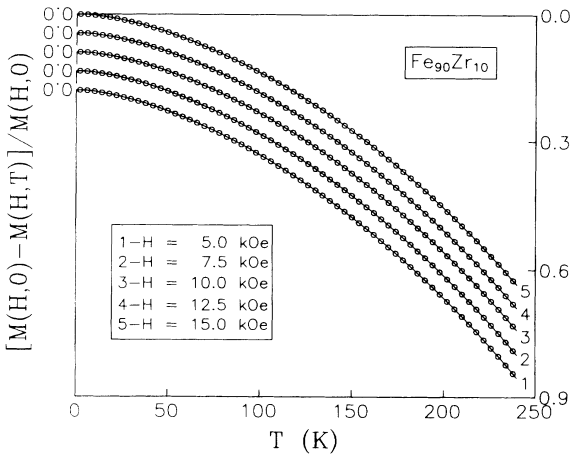

FIG. 2. $\Delta m(H,T)$ vs T measured at different fixed values of H. The least-squares fits to the data (see text) are shown as continuous curves.

$$D(T)=D_0(1-D_2T^2) \tag{7}$$

and

$$D(T)=D_0(1-D_{5/2}T^{5/2}) \tag{8}$$

in the case of itinerant- and localized-electron models, respectively. An elaborate data analysis, which makes use of Eqs. (1), (2), (3a), or (3b) and involves the combinations $D(T)=D_0$, $D(T)=D_0(1-D_2T^2)$, and $D(T)=D_0(1-D_{5/2}T^{5/2})$ with either $\beta=S=0$ or $\beta=0$, $S\neq 0$ or $\beta\neq 0$, $S=0$, and whose details are given in our earlier publications,[5,44] reveals that the expression that combines Eqs. (1), (2), (3b), and (7) and sets $\beta=0$ in Eq. (2) reproduces the $\Delta m(T)$ to the highest degree of accuracy for $T\lesssim 0.95T_C$. The optimum values of the parameters that yield the best theoretical fit (depicted by the continuous curves in Fig. 2), as inferred from the least value for the sum of deviation squares, χ^2, are $D_0=32(1)$ meV Å^2, $D_2=[1.5(1)]\times 10^{-6}$ K^{-2}, $D_{5/2}=\beta=0$, and $S=[1.1(2)]\times 10^{-6}$ K^{-2}. Contrasted with the *weak* field dependence of the upper limit of the temperature range over which such a theoretical fit adequately describes $\Delta m(T)$, the parameter values mentioned above do *not depend* on H. The above observations, including the presently determined parameter values, conform very well with the results of our recent magnetization measurements[5] on the a-$Fe_{90}Zr_{10}$ alloy sample belonging to a batch different from the present one.

Figure 3 shows $M^2(H,T)$ plotted again $H/M(H,T)$ at a few selected temperature values in the range 4.2–300 K. The M^2 vs H/M isotherms (Arrott plot isotherms) are *roughly* linear at high fields ($H\gtrsim 4$ kOe) for temperatures well outside the critical region ($\approx T_C\pm 10$ K). By contrast, the Arrott plot isotherms present a slight but finite curvature even at fields as high as 15 kOe in the critical region (note that such a curvature is not apparent for the isotherm taken at $T_C\simeq 240$ K in Fig. 3 because of the insensitive ordinate scale). Curvature in the high-field portion of the M^2 vs H/M isotherms makes an accurate determination of spontaneous magnetization, $M(0,T)$, impossible because an extrapolation of these

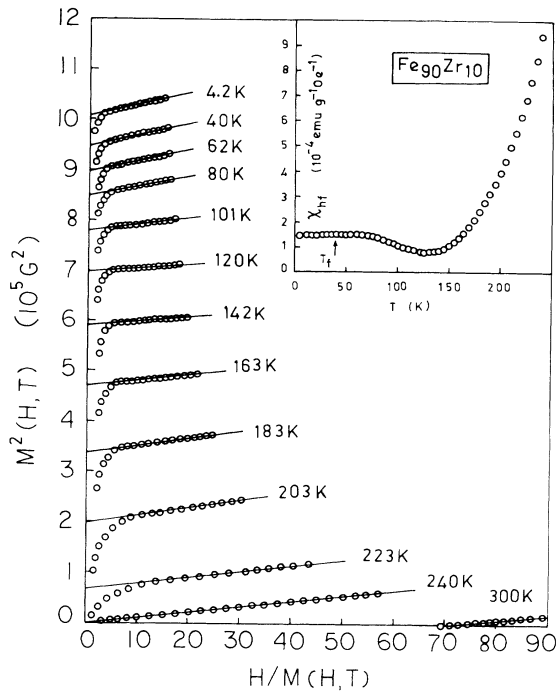

FIG. 3. $M^2(H,T)$ vs $H/M(H,T)$ isotherms. The inset shows the high-field magnetic susceptibility plotted against temperature.

high-field portions to zero field cannot be carried out unambiguously. To tackle this problem effectively, the isotherms are made exactly linear over a wide range of fields, especially in the high-field region, by allowing the critical exponents β and γ for $M(0,T)$ and initial susceptibility in the *modified* Arrott plot of $M^{1/\beta}$ against $(H/M)^{1/\gamma}$ to vary with temperature such that they assume 3D Heisenberg-like values[4] ($\beta\simeq 0.36$, $\gamma\simeq 1.38$) in the critical region and mean-field values ($\beta=0.5$, $\gamma=1.0$) for temperatures well outside the critical region. These high-field straight-line portions are then linearly extrapolated to $(H/M)^{1/\gamma}=0$ in order to arrive at accurate values of $M(0,T)$ for $T\lesssim T_C$. The $M(0,T)$ data so obtained are plotted as $[M(0,T)/M(0,0)]^2$ against T^2 and $M(0,T)/M(0,0)$ against $T^{3/2}$ in Fig. 4. It is evident from this figure that the thermal demagnetization of $M(0,T)$ at low temperatures occurs in accordance with the Bloch $T^{3/2}$ law, whereas the expression $[M(0,T)/M(0,0)]^2\cong 1-AT^2$ forms a much better description of the $M(0,T)$ data over a wide range of intermediate temperatures. A detailed analysis,[5,44] however, demonstrates that

$$M(0,T)/M(0,0)=[g\mu_B\xi(\tfrac{3}{2})/M(0,0)]\times[k_BT/4\pi D_0(1-D_2T^2)]^{3/2} \tag{9}$$

for $0\lesssim T\lesssim 0.25T_C$ with $g=2.07(2)$ (Ref. 24), $M(0,0)=1015(50)$ G, $D_0=26.5(20)$ meV Å^2, and $D_2=1.55(25)\times 10^{-6}$ K^{-2},

$$[M(0,T)/M(0,0)]^2=0.97(1)-[1.80(1)]\times 10^{-5}T^2 \tag{10}$$

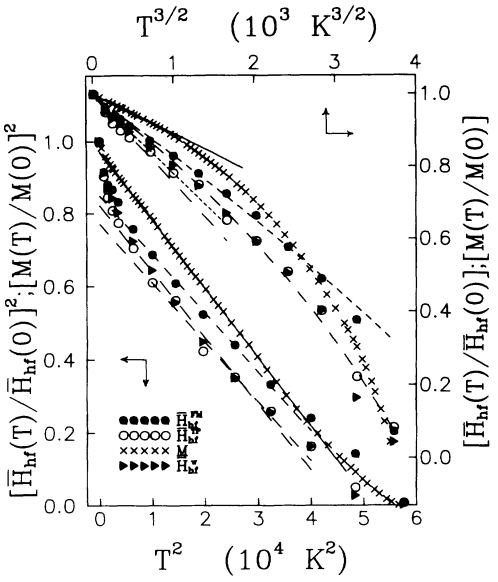

FIG. 4. Reduced magnetization $m(T)\equiv M(T)/M(0)$, and reduced average magnetic hyperfine fields, $h(T)\equiv\bar{H}_{hf}(T)/\bar{H}_{hf}(0)$, plotted against $T^{3/2}$, and the plots of $m^2(T)$ and $h^2(T)$ vs T^2. The curves drawn through the data points denote the best least-squares fits attempted in different temperature ranges based on Eqs. (9)–(11) of the text.

for $0.38T_C \lesssim T \lesssim 0.88T_C$ and

$$[M(0,T)/M(0,0)]^2 = 1.005(2) - [6.75(5)]\times 10^{-4}T^{4/3} \tag{11}$$

for $0.89T_C \lesssim T \lesssim 0.98T_C$. The least-squares fits (9) and (10) are respectively represented by the continuous curve and the straight line drawn through the data points (crosses) in Fig. 4. The data presented in Fig. 3 also demonstrate that magnetization does not saturate in fields up to 15 kOe at low temperatures; the high-field differential susceptibility just above the technical saturation, χ_{hf}, has a value $[15.0(5)]\times 10^{-5}$ emu g^{-1} Oe^{-1} at 4.2 K and increases steeply for $T > 150$ K to attain a value of $[94.0(10)]\times 10^{-5}$ emu g^{-1} Oe^{-1} at T_C (inset of Fig. 3). Of all the theoretical treatments[5,44,45] which overcome the major deficiencies in the conventional Stoner model, only the model proposed by Lonzarich and Taillefer[46] for ferromagnetic metals with *unsaturated* moments, which includes the corrections of the Stoner model arising from the *transverse* as well as *longitudinal local*-spin-density fluctuations and incorporates a natural temperature-dependent cutoff wave vector for the thermally excited modes, provides a straightforward explanation for the above observations by predicting a magnetic equation of state of the form

$$H = a(T)M(H,T) + bM^3(H,T) \tag{12}$$

valid in FM as well as PM regimes at large field strengths only and the temperature dependence of spontaneous magnetization of the type

$$[M(0,T)/M(0,0)] \simeq 1 - BT^{3/2} \tag{13}$$

at very low temperatures,

$$[M(0,T)/M(0,0)] \simeq [1-(T/T_C)^2]^{1/2}, \tag{14}$$

over a wide range of intermediate temperatures and

$$[M(0,T)/M(0,0)] = [1-(T/T_C)^{4/3}]^{1/2} \tag{15}$$

for temperatures close to T_c. A comparison between Eqs. (11) and (15) reveals that $T_C = 238.8(12)$ K, a value that agrees well with $T_C = 240(1)$ K deduced from the low-field magnetization data and also with $T_C = 238.50(5)$ K determined[25] from the bulk magnetization (BM) and ferromagnetic resonance (FMR) data taken in the critical region on the a-$Fe_{90}Zr_{10}$ sample coming from the same batch as the present one. From the foregoing remarks and the fact that Stoner single-particle excitations also manifest themselves in a temperature variation of $M(0,T)$ of the form given by Eq. (14), we conclude[5] that (i) the dominant contribution to $M(0,T)$ arises from spin-wave excitations for $T \lesssim 0.25T_C$, single-particle excitations and *local*—spin-density fluctuations for $0.38T_C \lesssim T \lesssim 0.88T_C$ and enhanced fluctuations in the *local* magnetization for $0.89T_C \lesssim T \lesssim 0.98T_C$; (ii) external fields $H \gtrsim 5$ kOe suppress the *local*- spin-density fluctuations completely, and hence the temperature dependence of $M(H,T)$ is solely governed by the spin-wave and single-particle excitations for temperatures up to $0.95T_C$; (iii) D is *independent* of H and renormalizes with temperature according to the expression given by the itinerant-electron model; and (iv) the softening of spin-wave modes takes place for $T \lesssim 60$ K ($\simeq 1.5T_f$).

Next, we focus our attention on the $\chi_{hf}(T)$ data presented in the inset of Fig. 3. This so-called "single-domain" susceptibility falls rapidly as the temperature is lowered below T_C and goes through a minimum at $T \simeq 130$ K before attaining a constant value for $T \lesssim 75$ K. In a conventional local-moment ferromagnet, $\chi \equiv dM/dH$ above technical saturation is expected to drop continuously to zero as $T \to 0$ K. Contrasted with this behavior, $\chi_{hf}(T)$, in the case of a weak itinerant ferromagnet, would exhibit a steep fall for temperatures just below T_C and as the temperature is lowered towards 4.2 K, the rate of decrease in $\chi_{hf}(T)$ should progressively slow down so that $\chi_{hf}(T)$ reaches a plateau at low temperatures without going through a minimum. Now that the alloy in question possesses all the properties of a weak itinerant ferromagnet[2,3,5,26] and ample experimental evidence[1,2,5,8–13,15,16,18–28] exists for the occurrence of a "mixed" magnetic phase (itinerant ferromagnetism coexists with spin-glass-like order) for $T < T_f$, the main contributions to $\chi_{hf}(T)$ for $T < T_f$ should arise from the Pauli spin paramagnetism and Van Vleck orbital paramagnetism of the d electrons belonging to the ferromagnetic phase and from the frozen transverse spin components or (AFM or FM) spin clusters. In view of these arguments, the minimum in $\chi_{hf}(T)$ at $T \simeq 130$ K should mark the onset of freezing. This inference suggests that the "transition" at T_f may not be as sharply defined as it is made out to be in the literature[9,10,12,18] and that the freezing process is *gradual* in the sense that it takes place over a wide range of temperatures.

B. Mössbauer effect

Zero-field ^{57}Fe Mössbauer effect (ME) spectra taken at various fixed values of temperature in the range 5–300 K are shown in Fig. 5(a). Two different methods of analysis have been used for the reasons explained below.

Optimum but *average* values of the intensity ratio b (defined as $I_{1,6}:I_{2,5}:I_{3,4}=3:b:1$), FWHM of the subspectral lines Γ, isomer shift δ and α, a direct measure of the linear correlation[47]

$$\delta(H_{\rm hf})=\delta(H^0_{\rm hf})-\alpha(H_{\rm hf}-H^0_{\rm hf}) \tag{16}$$

between the *local* isomer shift and the *local* hyperfine field, as well as the probability distribution of the magnetic hyperfine fields $P(H_{\rm hf})$ have been determined for each ME spectrum, using the Window method,[48] by following the procedure suggested by Keller.[49] A correlation between δ and $H_{\rm hf}$ of the type given by Eq. (16) had to be used in order to reproduce the observed asymmetry [Fig. 5(a)] in the lines. The values for the parameters b, Γ, and δ as well as for $\bar{H}^W_{\rm hf}$ (average hyperfine field), evaluated from $P(H^W_{\rm hf})$, obtained in this way at different temperatures for $N=8$ [this value of N is regarded as the most appropriate value based on our observation that $N<8$ obscures certain genuine details in $P(H_{\rm hf})$, whereas $N>8$ gives rise to unphysical structure in $P(H_{\rm hf})$ because a larger than required number of coefficients in the Fourier series tend to fit the statistical fluctuations in the measured spectrum], where N denotes the number of terms in the Fourier expansion, are displayed in Fig. 6 while the corresponding $P(H^W_{\rm hf})$-vs-$H_{\rm hf}$ curves at a few selected values of temperature are depicted in Fig. 7. The values for all the parameters are found to be *insensitive* to the choice of N in the interval $8\le N\le 12$, but specious structure develops at low fields in $P(H_{\rm hf})$ with increasing N due to the statistical scatter in the spectrum. Regardless of the value of N, the low-field tail in $P(H^W_{\rm hf})$ extends to $H_{\rm hf}=0$, particularly for the spectra taken at $T\cong T_C$. Now that a finite probability even at $H_{\rm hf}=0$ is known[49] to yield wrong values for the parameters, the results of Window analysis for $T\cong T_C$ should be regarded with caution.

Since the Window analysis does not make any provision for the spatial segregation of the sort envisaged in the spin-clusters–FM-matrix pictures (see Sec. I), the results obtained through this analysis cannot provide a rigorous test for the predictions based on these models. With a view to overcome this limitation of the Window method, two *independent* subspectra (each comprising six Lorentzian-shaped lines), characterized by two *distinctly different* but *average* values of b, Γ, δ, α, and $H_{\rm hf}$, are fitted to each of the measured spectra. Such a two-pattern fit is intended to describe the *local* magnetic order either for the widely different local environments corresponding to the "Fe-rich" and "Fe-poor" regions in the AFM-clusters–FM-matrix model (see Sec. I) or for the two *nonequivalent* Fe "sites" representing the spin locations within the *finite* FM spin clusters (for which the *local* magnetization $M_{\rm loc}$ is *lower* than that in the FM matrix) and the *infinite* FM matrix (for which $M_{\rm loc}$ is large). At discrete $H_{\rm hf}$ values (2 kOe apart) along the abscissas

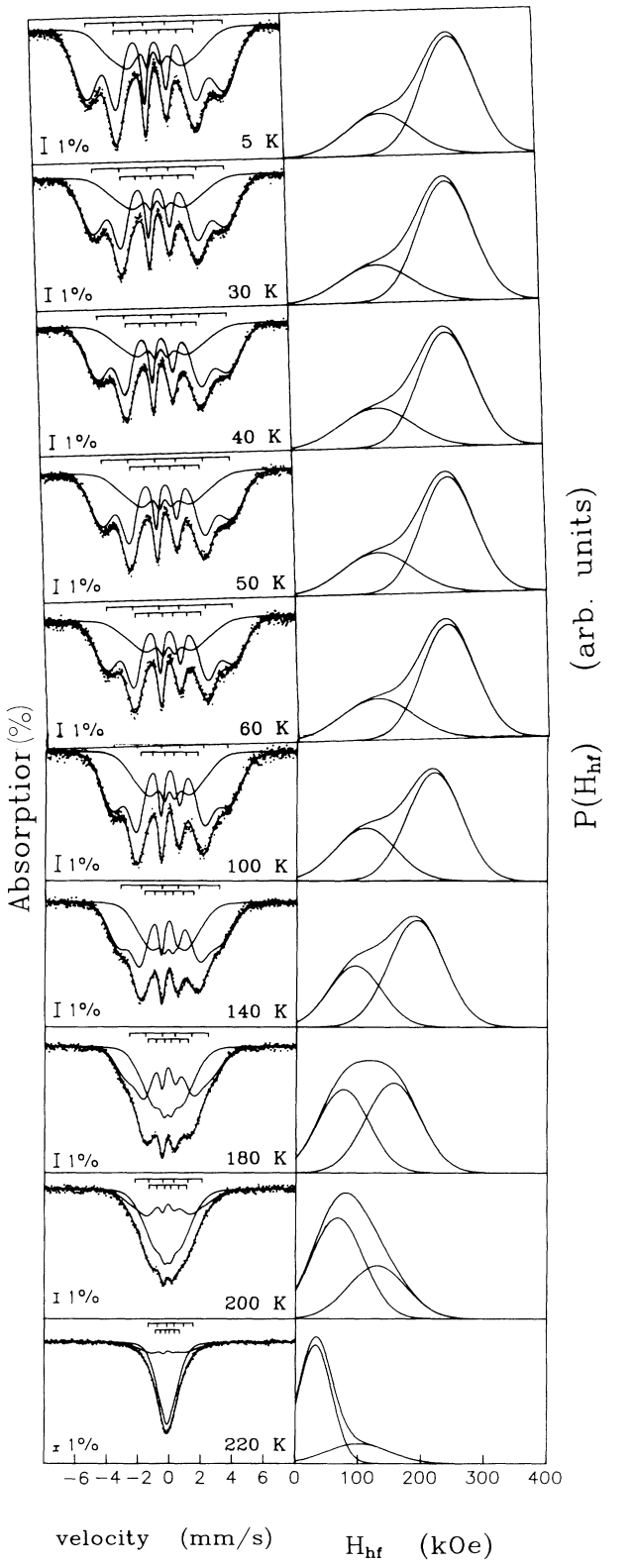

FIG. 5. (a) Mössbauer spectra at a few representative temperatures together with the best two-Gaussian fits, the subspectra sextets of Lorentzian lineshape, and their line positions. (b) The corresponding component Gaussian distributions and their resultant distribution.

of the $P(H_{hf})$-vs-H_{hf} Gaussian-shaped curves, individual Mössbauer spectra were calculated and added to form a resultant pattern for comparison with the experimental ME spectrum at each temperature ($T \lesssim T_C$). The optimum values of the above parameters for each subspectrum, arrived at by minimizing χ^2, the sum of squares of the deviations of the measured data points from the corresponding values calculated following the above procedure, are also shown in Fig. 6 (note that $\alpha(T)$ for both Window and two-pattern fits is not shown in this figure as it remains essentially constant at $\alpha^W=[5(2)]\times10^{-4}$, $\alpha^{cl}=[4.5(24)]\times10^{-4}$, and $\alpha^{FM}=[8.5(15)]\times10^{-4}$ in units of mm s^{-1} (kOe)$^{-1}$ for $T \lesssim T_c$). The best theoretical least-squares fits to the spectra so obtained are shown in Fig. 5(a) together with the subspectra and their line positions, while the resultant hyperfine-field distributions, $P(H_{hf}^{TP})$, used to generate these theoretical fits and their component Gaussian distributions are depicted in Fig. 5(b). The quality of the two-pattern (TP) fits is decidedly superior to that of the Window (W) fits at all temperatures as inferred from the value of χ^2 [Fig. 6(e)], which is corrected for the number of free-fitting parameters. The peak positions of the two-Gaussian distributions corresponding to the peak values of the low- and high-field components of $P(H_{hf})$ (or the ME spectrum) are identified with the average hyperfine fields for the clusters and the FM matrix, respectively, and denoted by $\bar{H}_{hf}^{cl}$ and $\bar{H}_{hf}^{FM}$ in Figs. 4 and 9, which also show temperature variation of the average hyperfine field for the main spectrum, $\bar{H}_{hf}^{TP}(T)$, computed from $P(H_{hf}^{TP})$. To facilitate a comparison between $P(H_{hf}^{TP})$ and $P(H_{hf}^{W})$, $P(H_{hf}^{W})$ for $N=8$ has also been fitted to the sum of two *independent* Gaussian distribution and the result is shown in Fig. 7 as the continuous curves. Note that the superscripts W and TP are used to denote the values of different ME parameters deduced from the observed ME spectra using the Window and the two-pattern methods, respectively.

The variation of the *reduced* average hyperfine fields $\bar{H}_{hf}^{W}$, $\bar{H}_{hf}^{TP}$, $\bar{H}_{hf}^{FM}$, and $\bar{H}_{hf}^{cl}$ with temperature has been ana-

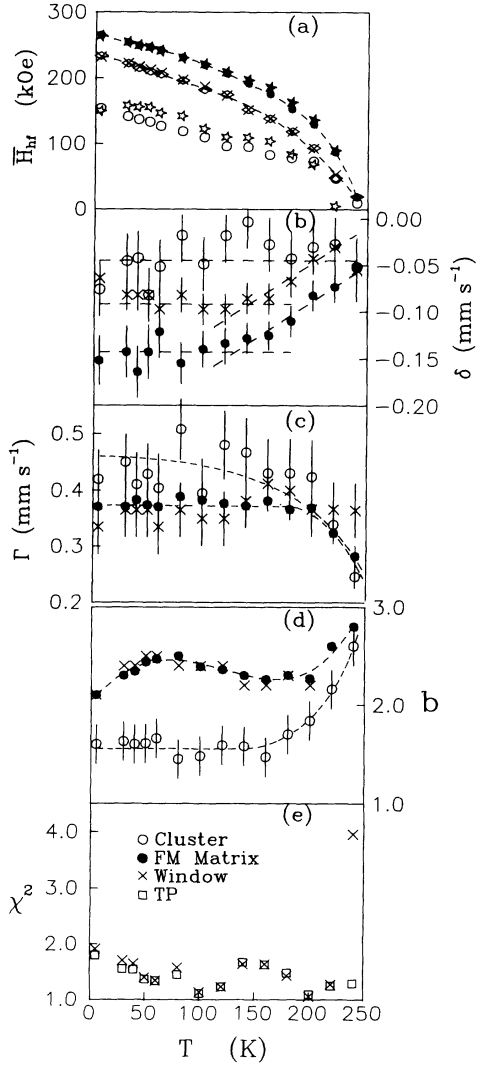

FIG. 6. Temperature dependence of the Mössbauer parameters (a) $\bar{H}_{hf}^{W}$(×), the most probable hyperfine fields corresponding to the two-Gaussian components (Fig. 7) [high-field (★); low-field (☆)] of $P(H_{hf}^{W})$, $\bar{H}_{hf}^{TP}$ (◇), $\bar{H}_{hf}^{cl}$ (○), and $\bar{H}_{hf}^{FM}$ (●); (b) δ^W(×), δ^{cl} (○), δ^{FM} (●); (c) Γ^W(×), Γ^{cl} (○), Γ^{FM} (●); (d) b^W(×), b^{cl} (○), b^{FM} (●); and of the reduced χ^2 (e) χ^2_W (×), χ^2_{TP} (□), deduced from the window ($N=8$) and TP fits.

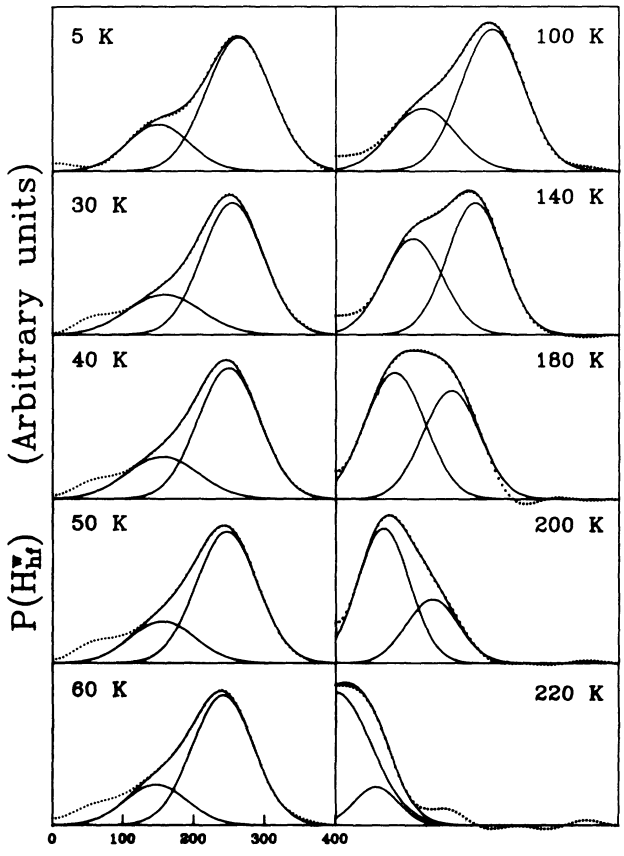

FIG. 7. $P(H_{hf}^{W})$ vs H_{hf} for $N=8$. The two-Gaussian fits to the $P(H_{hf}^{W})$-vs-H_{hf} curves are shown by the continuous curves.

lyzed in terms of the expressions of the form given by Eqs. (9)–(11), in which the quantity $M(0,T)/M(0,0)$ on the left-hand side is replaced by $\bar{H}_{\rm hf}(T)/\bar{H}_{\rm hf}(0)$, with the following results.

(i) Unlike the reduced magnetization data, the $\bar{H}^{W}_{\rm hf}(T)/\bar{H}^{W}_{\rm hf}(0)$ $[\bar{H}^{\rm TP}_{\rm hf}(T)/\bar{H}^{\rm TP}_{\rm hf}(0)$, $\bar{H}^{\rm FM}_{\rm hf}(T)/\bar{H}^{\rm FM}_{\rm hf}(0)]$ data can be successfully fitted to Eq. (9) in *two* different temperature ranges, i.e., in $0 \lesssim T \lesssim 0.21T_C$ with the choice of the parameters $M(0,0)=1000(1)$ [1001(4), 1000(3)] G, $D_0=24(2)$ [22(2), 25.5(20)] meV Å^2, and $D_2 \simeq 0$, and within $0.17T_C \lesssim T \lesssim 0.92T_C$ with $M(0,0)=1000(3)$ [1000(3), 1000(3)] G, $D_0=29(2)$ [28(2), 31(2)] meV Å^2, and $D_2=[2.36(110)]\times 10^{-6}$ $\{[2.3(11)]\times 10^{-6}, [2.1(11)]\times 10^{-6}\}$ K^{-2}, respectively.

(ii) In the temperature range $0.33T_C \lesssim T \lesssim 0.75T_C$, the expression $[\bar{H}_{\rm hf}(T)/\bar{H}_{\rm hf}(0)]^2 = A - BT^2$ could also form a reasonable description of the temperature dependence of the quantities mentioned in (i), but Eq. (9) provides a decidedly better fit to the $\bar{H}^{W}_{\rm hf}(T)$, $\bar{H}^{\rm TP}_{\rm hf}(T)$, and $\bar{H}^{\rm FM}_{\rm hf}(T)$ data, denoted by solid triangles, open circles, and solid circles in Fig. 4.

(iii) All the expressions mentioned above fail to describe the $\bar{H}^{\rm cl}_{\rm hf}(T)$ shown in Fig. 9.

Another important result is that the observed ME spectra could not be fitted on the assumption that either a single-Gaussian distribution or three such distributions constitute $P(H_{\rm hf})$. While the single-Gaussian fits could not account for the low-field part of the spectra, in particular, the three-Gaussian fits, even with a larger number of free-fitting parameters, did not lead to any significant improvement in the quality of the fits compared to that achieved by the two-Gaussian fits. Thus, we conclude that the ME spectrum at any given temperature ($T \lesssim T_C$) for the glassy alloy in question is adequately described by the sum of two independent subspectra computed from the two-Gaussian distributions [low- and high-field components of $P(H_{\rm hf})$].

1. *Hyperfine-field distribution*

The hyperfine-field distribution curves, $P(H^{\rm TP}_{\rm hf})$ in Fig. 5(b) and $P(H^{W}_{\rm hf})$ in Fig. 7, demonstrate the existence of a bimodal structure in $P(H_{\rm hf})$ for all the temperatures below T_C since the presence of a low-field component in them is clearly noticed. This low-field component, however, does not manifest itself as a well-resolved peak as is normally the case with bimodal distributions, but appears more as a shoulder on the low-field side of the main peak. In conformity with the present findings and those reported previously[6–9,11,13–15,37] by other workers, Ryan and Ren[16] observe a low-field shoulder in $P(H_{\rm hf})$ at all temperatures below T_C, but they dismiss its existence on the pretext that the statistical fluctuations in the central region of the Mössbauer-effect (ME) spectra give rise to this specious effect. As already mentioned, the statistical fluctuations in the measured spectra are reflected in $P(H_{\rm hf})$ only when the number of terms in the Fourier expansion used for the evaluation of $P(H_{\rm hf})$ greatly exceeds the optimum value of N. Moreover, a close scrutiny of the residual plots (Fig. 1 of Ref. 16) reveals that the Window fits of Ryan and Ren[16] do not account for the low-field part (the range of velocities embracing the zero-velocity region) of their ME spectra and hence the low-field component of $P(H_{\rm hf})$ has been underestimated. An unequivocal evidence for a bimodal $P(H_{\rm hf})$ in *a*-$Fe_{90+x}Zr_{10-x}$ alloys is provided by the bimodal frequency distribution of the spin-echo amplitude[26] and by our observation that neither a single-Gaussian distribution nor three-Gaussian distributions, but only two-Gaussian distributions form an adequate description of the observed ME spectra and hence of $P(H_{\rm hf})$. An observation similar to that just mentioned regarding the bimodal character of $P(H_{\rm hf})$ has also been made by Morrish *et al.*[50] on *a*-$Fe_{92}Zr_8$. Only the models that postulate a spatially segregated coexistence of finite spin clusters and FM matrix, but not the TSF model which insists on a microscopically homogeneous nature of the magnetic ordering, can provide a straightforward explanation for a bimodal $P(H_{\rm hf})$. Within the framework of such models, the low- and high-field peaks in $P(H_{\rm hf})$ originate from the spin clusters and FM matrix, respectively. In view of the finding that a sum of two-Gaussian distributions adequately describes both $P(H^{\rm TP}_{\rm hf})$ as well as $P(H^{W}_{\rm hf})$ (barring the structure with very low probability in weak fields particularly at low temperatures which is an artifact of the Window analysis), the areas under the low- and high-field Gaussian curves normalized to the total area under the $P(H_{\rm hf})$-vs-$H_{\rm hf}$ curve give the fraction of spins belonging to the clusters [low-field spin (LFS) fraction] and to the FM matrix [high-field spin (HFS) fraction], respectively. However, it should be recalled that the two-Gaussian fits yield more reliable estimates for LFS and HFS fractions because these fits reproduce the observed spectra with much higher accuracy than the Window fits. The temperature dependence of the LFS and HFS fractions so determined is shown in Fig. 8. It is evident from this figure that the LFS fraction increases at the expense of the HFS fraction as the temperature is raised beyond $T^* \simeq 150$ K and amounts to about 90% of the total Fe spins at $T \simeq T_C$. Now that both the AFM-spin-clusters–FM-matrix (AFM-FM) and the FM-spin-clusters–plus–FM-matrix (FM-FM) models are capable of explaining a bimodal $P(H_{\rm hf})$, it is imperative to find out which of these models yields a variation of LFS and HFS with temperature that is consistent with the one borne out by the present experiments. In the former model, the spin clusters are Fe-rich regions in which Fe spins are antiferromagnetically coupled as in fcc γ-Fe so that the LFS fraction is expected to remain essentially constant for temperatures well below the cluster Néel temperature ($T_N \simeq 70$ K for $^{14}\gamma$-Fe) and *decrease* at an increasingly faster rate when the temperature is raised well above T_N because the spins within cluster are completely disordered for $T > T_N$ ($T^{\rm cl}_N \ll T^{\rm FM}_C$) and get easily polarized by the spins belonging to the FM matrix. The attendant changes that should occur in $P(H_{\rm hf})$ are as the temperature is increased through T_N, the low-field Gaussian peak should narrow down and its peak position shift to lower fields as $T \rightarrow T_N$ such that the area under this peak, i.e., the LFS fraction, remains essentially unaltered in the

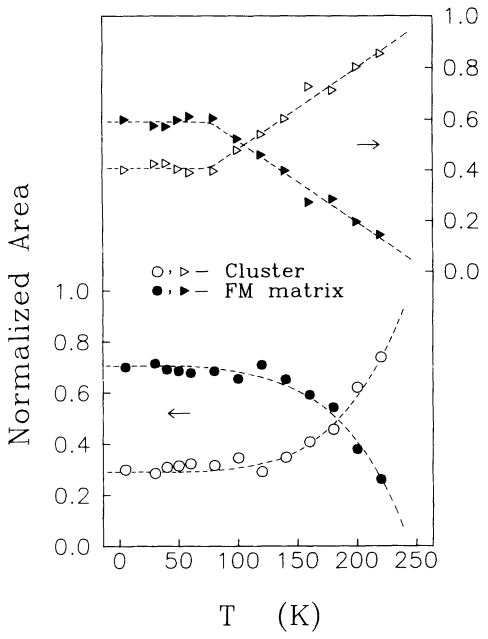

FIG. 8. Temperature dependence of the normalized area under the low-field Gaussian curve, "low-field spin fraction" [Window (△); two-Gaussian (○)] and under the high-field Gaussian curve, "high-field spin fraction" [Window (▲); two-Gaussian (●)].

initial stages of this process and then rapidly broaden out at temperatures well above T_N. As a consequence, the two peaks in $P(H_{hf})$ should become better resolved as $T \rightarrow T_N$ (considering the fact that the high-field peak hardly changes its position in this temperature range) and the low-field Gaussian peak should appear more as a shoulder to the main high-field peak for temperatures well above T_N. None of these trends is noticed either in the $P(H_{hf})$ [Figs. 5(b) and 7] or in the LFS-fraction–vs–T curve (Fig. 8). According to Read *et al.*,[14] the above model provides an alternative means of determining the LFS fraction from the zero-velocity Mössbauer absorption, $A_0(T)$, data taken at various temperatures, as elucidated below. At very low temperatures ($T \ll T_N \simeq 70$ K), the spins constituting the AFM clusters as well as those forming the FM matrix are in a magnetically ordered state, whereas for $T > T_N$ (e.g., $T = 80$ K) the cluster spins are disordered, giving rise to a paramagnetic absorption at such temperatures, while the FM spins continue to remain in the ordered state. At $T > T_C$, all Fe atoms are paramagnetic so that the ratio $[A_0(80\text{ K}) - A_0(300\text{ K})]/A_0(300\text{ K})$ should correspond to the LFS fraction. The value of this ratio calculated from the zero-velocity absorption (ZVA) data shown in Fig. 1 (note that the values of T_C deduced from the ZVA and low-field magnetization data taken on the same *a*-$Fe_{90}Zr_{10}$ sample match exactly) comes out to be $\simeq 0.19$. A comparison of this value with the estimate 0.30 given by the TP method (Fig. 8) underlines the futility of the approach adopted by Read *et al.*[14] To elucidate this point further, the ZVA data shown in Fig. 1 make it amply clear that the value of the LFS fraction deduced from such data crucially depends on the value of T_N assumed (there is no *a priori* reason to believe that the Néel temperature for the AFM clusters should be the same as that of γ-Fe) particularly when $T_N \gtrsim 150$ K; in the latter case, the higher the value of T_N (compared to 150 K), the lower the LFS fraction and the larger the discrepancy between the values of the LFS fraction obtained from the ZVA data and TP analysis. In any case, the AFM-FM model yields a variation of the LFS fraction with temperature that is in direct contradiction with the one presented in Fig. 8. Inadequacy of this model to describe the nature of magnetic ordering in *a*-$Fe_{90+x}Zr_{10-x}$ alloys correctly is also evident from the earlier observation[6,13,50] that the positions of the low-field and high-field Gaussian peaks both decrease in direct proportion to the applied magnetic field. By contrast, the FM-FM model predicts the temperature variation of the LFS and HFS fractions correctly in that the exchange interaction between spins in the FM matrix weakens as $T \rightarrow T_C$ while the FM coupling between the spins within the finite clusters is still quite strong due to the higher Curie temperature for the clusters so that the cluster spins polarize an increased number of spins originally belonging to the FM matrix and grow in size at the expense of the FM matrix. The results of our recent FMR measurements[22–25] on *a*-$Fe_{90+x}Zr_{10-x}$ alloys lend further support to this interpretation. Moreover, the present finding that only about 10% of the total Fe spins in *a*-$Fe_{90}Zr_{10}$ constitute the FM matrix for temperatures in the immediate vicinity of T_C is consistent with our observation,[25] based on BM and FMR measurements in the critical region, that only 11% of the total Fe spins are actually participating in the FM-PM phase transition for this glassy alloy. Recognizing that the Curie temperature for the FM clusters greatly exceeds the bulk T_c and that the relaxation time of the clusters, τ_{cl}, is much larger than the ^{57}Fe Mössbauer measurement time $\tau \simeq \hbar/\Gamma \approx 10^{-7}$ s, where Γ is the resonance linewidth of the Mössbauer transition, at all temperatures ranging from 4.2 K to $T \simeq T_C$, the observation that the bimodal structure in $P(H_{hf})$ persists to temperatures as high as T_C is in consonance with SANS evidence[29] for huge (200–400 Å) static clusters which do not disorder at T_C and also with the existence of giant "superparamagnetic-like" clusters for temperatures well above T_C, as inferred from earlier BM (Refs. 2, 4, and 7) and Mössbauer[13] results. Contrary to this behavior, a paramagnetic contribution to Mössbauer spectra is expected for $T > T_N$, which lies well below T_C, in the case of the AFM-FM model.

2. *Hyperfine fields*

The main points that emerge from the analysis of the temperature dependence of the average hyperfine fields $\bar{H}_{hf}^{W}$, $\bar{H}_{hf}^{TP}$, $\bar{H}_{hf}^{cl}$, and $\bar{H}_{hf}^{FM}$ [Figs 4 and 6(a)] are (i) the spin-wave excitations are mainly responsible for $\bar{H}_{hf}^{W}(T)$, $\bar{H}_{hf}^{TP}(T)$, and $\bar{H}_{hf}^{FM}(T)$ in the range $T \lesssim 0.2T_C$ where these quantities as well as $M(0,T)$ yield the same value, $D_0 \simeq 24$ meV Å^2, for the spin-wave stiffness coefficient; (ii) over a wide range of intermediate temperatures ($0.2T_C \lesssim T \lesssim 0.9T_C$), D_0 possesses a higher value

($D_0 \simeq 32$ meV Å^2); and (iii) the hyperfine fields mentioned above, instead of following the temperature dependence of $M(0,T)$ as is normally expected, mimic the temperature variation of the spontaneous magnetization extracted from the $M(H,T)$ data, as explained below. Figure 9 compares $\bar{H}_{\rm hf}^{W}(T)$, $\bar{H}_{\rm hf}^{\rm TP}(T)$, $\bar{H}_{\rm hf}^{\rm FM}(T)$, and $\bar{H}_{\rm hf}^{\rm cl}(T)$ with $M(0,T)$ and $M'(0,T)$, where $M(0,T)$ denotes the spontaneous magnetization data obtained through an extrapolation of the $M^{1/\beta}$ vs $(H/M)^{1/\gamma}$ isotherms (Sec. III A) whereas $M'(0,T)$ signifies the spontaneous magnetization data generated using the optimum parameter values [$M(0,0)=1006$ G, $D_0=32$ meV Å^2, $D_2=1.5\times10^{-6}$ K^{-2}, and $S=1.1\times10^{-6}$ K^{-2}] corresponding to the best least-squares fit to the "in-field" magnetization $M(H,T)$ data in the expression

$$M'(0,T)/M(0,0)=[g\mu_B\xi(\tfrac{3}{2})/M(0,0)] \times[k_BT/4\pi D_0(1-D_2T^2)]^{3/2}+ST^2 . \quad (17)$$

Such a comparison, besides reinforcing the above statement (iii), reveals a close agreement between $\bar{H}_{\rm hf}^{W}(T)$ and $\bar{H}_{\rm hf}^{\rm TP}(T)$. Recalling that the thermoremanent and thermomagnetic effects as well as the *local*- spin-density fluctuations are completely suppressed by fields $H \gtrsim 5$ kOe, the $M'(0,T)$ data, unlike the $M(0,T)$ data, do not make any allowance for the *local*-spin-density fluctuations as well as for the softening of the spin-wave modes for $T \lesssim 0.2T_C$ [indicated by the $M(0,T)$ and $H_{\rm hf}(T)$ data]. Thus, the shaded region in Fig. 9 depicts the contribution to thermal demagnetization due to the fluctuations in *local* magnetization. In view of the above remark, the observation that the temperature dependence of $\bar{H}_{\rm hf}^{W}$, $\bar{H}_{\rm hf}^{\rm TP}$, and $\bar{H}_{\rm hf}^{\rm FM}$ coincides only with $M'(0,T)$ but not with $M(0,T)$, far from implying a wide disparity between the results of local (Mössbauer) and bulk (magnetization) measurements, brings to attention the inadequacy of the Window and two-Gaussian-type methods to describe the ME spectra for a spin system in which the relaxation effects, arising from the *local* —spin-density (and hence hyperfine-field) fluctuations, are important. This limitation of the above methods stems from their underlying assumption that the spin correlation time $\tau_c \ll \tau$. Therefore, a more rigorous analysis of the ME spectra recorded on *a*-$Fe_{90+x}Zr_{10-x}$ alloys, in which τ_c is expected to be comparable to τ, than that attempted hitherto should include the effects on the line shape originating not only from a distribution of hyperfine fields caused primarily by the structural fluctuations in these *noncrystalline* materials but also from the fluctuations in the hyperfine fields. Such an analysis is not possible at present because the underlying theoretical framework is lacking. In this connection, it should be mentioned that stochastic model,[51] which calculates the ME line shape in the presence of a fixed axially symmetric electric-field gradient (EFG) and a magnetic hyperfine field which fluctuates randomly between the limits $+h$ and $-h$ and is directed either along or perpendicular to the axis of EFG, has been successfully used by Rancourt *et al.*[52] to describe the ME spectra in *crystalline* Fe-Ni Invar alloys. Since the magnitude of EFG has a distribution and EFG has no fixed direction in an amorphous alloy, this model is severely limited in scope so far as the ME lineshapes in the amorphous materials are concerned.

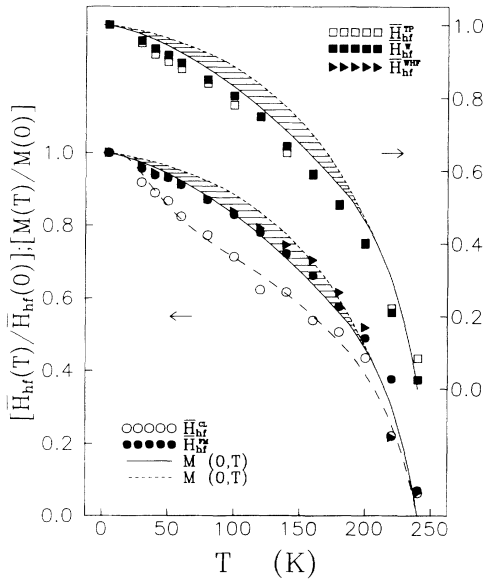

FIG. 9. Temperature dependence of $\bar{H}_{\rm hf}^{\rm TP}$ (□), $\bar{H}_{\rm hf}^{W}$ (■), $\bar{H}_{\rm hf}^{\rm cl}$ (○), $\bar{H}_{\rm hf}^{\rm FM}$ (●), $\bar{H}_{\rm hf}^{WHF}$ [▲, peak value of the high-field Gaussian component of $P(H_{\rm hf}^{W})$] and of $M(0,T)$ (small dashed curve) and $M'(0,T)$ (continuous curve). For the meaning of the above symbols, see text. The dashed curve drawn through the open circles represents the least-squares fit to the $\bar{H}_{\rm hf}^{\rm cl}(T)$ data based on Eqs. (18) and (19) with the choice of the parameters given in the text.

Another interesting aspect of the data displayed in Fig. 9 is that $\bar{H}_{\rm hf}^{\rm cl}(T)$ differs markedly from $M'(0,T)$. Recognizing that the temperature variation of $\bar{H}_{\rm hf}^{\rm cl}$ resembles that of the hyperfine fields of Mn impurities[53] in the Fe host, we adopt a theoretical approach similar to that of Callen, Hone, and Heeger[54] and of Wolfram and Hall[55] and approximate the *weak* coupling between the finite FM spin clusters and the infinite FM matrix by a molecular (exchange) field acting on the spin clusters (impurities) due to the spins in the FM matrix (host) with the result that the reduced hyperfine field $\bar{H}_{\rm hf}^{\rm cl}(T)/\bar{H}_{\rm hf}^{\rm cl}(0)$ is given by

$$\bar{H}_{\rm hf}^{\rm cl}(T)/\bar{H}_{\rm hf}^{\rm cl}(0)=B_s(y) \quad (18)$$

with

$$y=(g\mu_BH_{\rm ex}S/k_BT)[M'(0,T)/M(0,0)] =\lambda(T_C/T)[M'(0,T)/M(0,0)]$$

and

$$\lambda=g\mu_BH_{\rm ex}S/k_BT_C$$

where B_s is the Brillouin function corresponding to the spin S of the clusters, $[M'(0,T)/M(0,0)]$ is the reduced magnetization of the FM matrix, λ is the molecular-field coupling parameter, and $H_{\rm ex}$ is the exchange (molecular) field experienced by the spin clusters on account of the

FM matrix spins. An attempt to fit Eq. (18) to the $\bar{H}_{\rm hf}^{\rm cl}(T)/\bar{H}_{hf}^{\rm cl}(0)$ data using a nonlinear least-squares-fit computer program which treats λ as a free-fitting parameter reveals that Eq. (18) is incapable of producing the type of temperature variation observed unless λ is taken to be a temperature-dependent parameter. The best least-squares fit to the data based on Eq. (18), represented in Fig. 9 by the dashed curve, is obtained only when the temperature dependence of λ of the form

$$\lambda(T)=\alpha_0-\exp[-(T/T_0)^{\beta_0}] \tag{19}$$

is assumed and the parameters α_0, β_0, and T_0 take on the values $\alpha_0=1.32(3)$, $\beta_0=1.80(8)$, and $T_0=150(5)$ K. The stretched exponential form of $\lambda(T)$ is suggestive of the hierarchical nature of the exchange interaction between the spins contained within the clusters and those forming the FM matrix, and T_0 is a "characteristic" temperature beyond which the cluster-matrix exchange coupling picks up in strength at a more rapid rate. One could imagine such a situation to arise if there exist clusters within clusters such that with temperature increasing from 4.2 K, first the spins belonging to the largest cluster and then those constituting the smaller and smaller clusters are exposed to the exchange field of the FM matrix spins. In this picture, T_0 marks a temperature above which an increasing number of smaller clusters "feel" the presence of the FM matrix and grow in size at the expense of the FM matrix. This interpretation is consistent with that given to the increase in the LFS fraction with temperature in the preceding subsection.

With a view to gain further insight into the physical origin of the hyperfine fields in the glassy alloy under consideration, an effort is made to estimate the relative magnitude of the different contributions to $\bar{H}_{\rm hf}$. According to the commonly used phenomenological model, there are two *main* contributions to $\bar{H}_{\rm hf}$: $H_{\rm hf}^{\rm loc}=A\mu_L$, which accounts for the polarization of conduction-electron spins due to the on-site moment μ_L as well as for the polarization of inner s-shell (core) electrons by the localized $3d$-electron spins, and $H_{\rm hf}^{\Sigma}=B\bar{\mu}$, which arises on account of the polarization of the conduction-electron spins by the moments on the surrounding atoms, i.e.,

$$H_{\rm hf}=A\mu_L+B\bar{\mu}\ . \tag{20}$$

It is customary to plot $\bar{H}_{\rm hf}$ against $\bar{\mu}$ at the lowest temperature (mostly 4.2 K) either for various compositions in a given alloy series or for the amorphous alloys of a similar kind or crystalline compounds and estimate the coefficients A and B in Eq. (20) from the intercept on the ordinate and slope of the straight line, respectively. Instead of following this approach, we determine the values of A and B from the $\bar{H}_{\rm hf}(T)$-vs-$\bar{\mu}_{\rm Fe}(T)$ plot, calculated from the $M'(0,T)$ data, shown in Fig. 10. In this figure, the dashed straight line passing through the origin corresponds to the $H_{\rm hf}$-vs-$\mu_{\rm Fe}$ relationship found[56] in α-Fe. From Fig. 10, it is noticed that the coefficient B (slope) has nearly the same value ($B\simeq 155$ kOe/μ_B) for the average hyperfine fields, $\bar{H}_{\rm hf}^{\rm FM}(\bar{\mu})$, $\bar{H}_{\rm hf}^{\rm TP}(\bar{\mu})$, and $\bar{H}_{\rm hf}^{W}(\bar{\mu})$, in a-$Fe_{90}Zr_{10}$ as for $\bar{H}_{\rm hf}(\bar{\mu})$ in α-Fe, but unlike the $H_{\rm hf}(\mu_{\rm Fe})$ data the former sets of data yield a *finite intercept* on the ordinate. In view of a finite value of $H_{\rm hf}^{\rm loc}$, the usual practice[9,10,12] of using the conversion factor 150 kOe/μ_B, valid for α-Fe, for calculating the iron moment from the observed average hyperfine field for a-$Fe_{90+x}Zr_{10-x}$ alloys or even for other amorphous Fe-based ferromagnetic alloys can lead to erroneous results, as explained below. In the case of α-Fe at 4.2 K, $H_{\rm hf}^{\rm loc}=-200$ kOe, $H_{\rm hf}^{\Sigma}\simeq -145$ kOe (Ref. 56) and the moment at each site is the same so that $\mu_L=\bar{\mu}=2.212\mu_B$, the slope $B'=(A+B)\simeq 156$ kOe/μ_B, and $H_{\rm hf}(\bar{\mu}=0)=0$. Contrasted with this behavior, $H_{\rm hf}^{\rm loc}=22(6)$ [$-14(4)$] and $H_{\rm hf}^{\Sigma}=156(5)\bar{\mu}_{\rm Fe}$ [$155(5)\bar{\mu}_{\rm Fe}$] in units of kOe for $\bar{H}_{\rm hf}^{\rm FM}$ [$\bar{H}_{\rm hf}^{\rm TP}$ or $\bar{H}_{\rm hf}^{W}$] in a-$Fe_{90}Zr_{10}$ with $\bar{\mu}_{\rm Fe}=1.53\mu_B$ at 4.2 K, and the moment in this alloy, as in other compositions of the series a-$Fe_{90+x}Zr_{10-x}$, differs from site to site due to topological disorder. The above comparison demonstrates that $H_{\rm hf}^{\rm loc}$ is 1 order to magnitude smaller while $H_{\rm hf}^{\Sigma}$ is about 1.6 times *larger* in a-$Fe_{90}Zr_{10}$ than in α-Fe. The agreement between the values of $dH_{\rm hf}/d\bar{\mu}$ for a-$Fe_{90}Zr_{10}$ and α-Fe is, therefore, deceptive. Consequently, the values of $\mu_{\rm Fe}$ computed[9,10,12,13] from $\bar{H}_{\rm hf}$ using the above conversion factor cannot be considered as reliable and the discrepancy between the moment values so calculated and those directly measured used as an argument by some workers[9,13] for the existence of noncollinear magnetic structure in the ground state should be regarded with great caution. In this context, it is important to note that the estimate of $\simeq 0.7\mu_B$ for the moment corresponding to the low-field peak in $P(H_{\rm hf})$, calculated[8,9,13,26] from the value of $\bar{H}_{\rm hf}^{\rm cl}$ at 4.2 K following the above procedure and generally taken as evidence for the presence of γ-Fe regions in the amorphous FM matrix, does not make any sense in the light of the present finding that $\bar{H}_{\rm hf}^{\rm cl}$ *does not scale* with $\bar{\mu}_{\rm Fe}$. Moreover, this phenomenological model [Eq. (20)] is expected to find limited application so far as the systems in which local magnetization fluctuations govern the thermal demagnetization behavior are concerned.

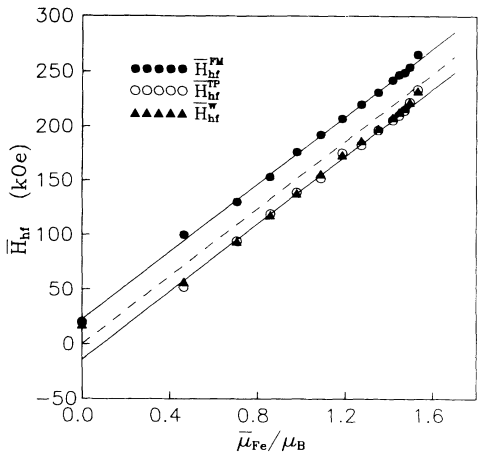

FIG. 10. Average hyperfine field $\bar{H}_{\rm hf}$ as a function of average magnetic moment on the Fe atom, $\bar{\mu}_{\rm Fe}$.

3. *Isomer shifts*

The *average* isomer shift δ for a-$Fe_{90}Zr_{10}$ relative to α-Fe at 300 K is plotted as a function of temperature in

Fig. 6(b). While $\delta^W(T)$ and $\delta^{FM}(T)$ remain constant at $\simeq -0.09(1)$ mm s^{-1} and $\simeq -0.143(21)$ mm s^{-1} for $T \lesssim 150$ K and increase roughly linearly with temperature for higher temperatures, $\delta^{cl} = -0.045(17)$ mm s^{-1} throughout the temperature range 5 K $\leq T \leq$ 240 K. As is well known, the temperature-dependent contribution to the isomer shift is caused by the time dilations resulting from the thermal motions of the γ-ray-emitting and -absorbing nuclei. This contribution, called the second-order Doppler (SOD) shift, is given by $\Delta E_\gamma / E_\gamma = -\langle v^2 \rangle / 2c^2$, where E_γ is the recoilless γ-ray energy, ΔE_γ is the shift in energy, v is the velocity of the emitting nucleus in the direction of the γ ray, and c is the velocity of light. In the harmonic approximation, the temperature dependence of the centroid of the ME spectrum in velocity units is given by

$$\delta v_T = -\frac{C_L}{2Mc}(T_a - T_s) , \tag{21}$$

where M is the atomic mass, C_L is the lattice specific heat, and T_a and T_s denote the temperature of the absorber and source, respectively. If both T_a and T_s lie well above the Debye temperature Θ_D (the high-temperature limit) $C_L \cong 3k_B$ (k_B is the Boltzmann constant), and δv_T is a linear function of temperature with slope $-3k_B/2Mc$. For ^{57}Fe, this slope has a value -7.2×10^{-4} mm s^{-1} K^{-1}. For a-$Fe_{90}Zr_{10}$, the least-squares fits in the temperature range 140 K $\lesssim T \lesssim$ 240 K (140 K $\lesssim T \lesssim$ 220K) yield the value $\partial\delta^{FM}(T)/\partial T = 7.4(3)\times10^{-4}$ mm s^{-1} K^{-1} [$\partial\delta^W(T)/\partial T = 7.4(3)\times10^{-4}$ mm s^{-1} K^{-1}]. The slope turns out to be *positive* since $T_a < T_s$ for temperatures up to $T_C \simeq 240$ K. A close agreement between the experimental and theoretical values of $\partial\delta(T)/\partial T$ indicates that the linear increase of $\delta(T)$ for $T \gtrsim 150$ K is due to the SOD shift.

4. Linewidth

$\Gamma^W(T)$, $\Gamma^{FM}(T)$, and $\Gamma^{cl}(T)$, displayed in Fig. 6(c), demonstrate that Γ^W has a temperature-independent value of 0.365(45) mm s^{-1} within the temperature region 5 K $\lesssim T \lesssim$ 240 K as contrasted with Γ^{FM} and Γ^{cl} which remain constant at $\Gamma^{FM} = 0.378(12)$ mm s^{-1} and $\Gamma^{cl} = 0.45(5)$ mm s^{-1} for $T \lesssim 200$ K, exhibit a steep fall above this temperature, and approach the intrinsic linewidth of the Fe source as $T \to T_C$. Note that the discrepancy between results of the Window and TP-fitting methods for $T \gtrsim 200$ K is of no serious consequence considering the inability of the former method to yield reliable results particularly for temperatures close to T_C. A rapid decline in the value of Γ as $T \to T_C$ is generally attributed[57] to the narrowing down of the distribution of magnetic moments (and hence of hyperfine fields) with increasing temperature due to long-range correlations between the individual magnetic moments. This interpretation is, however, strictly valid only when the distribution of hyperfine fields is the sole cause of broadening and in that case $\Gamma(T) \propto \bar{H}_{hf}(T)$. An inspection of Figs. 6(a) and 6(c) shows that such a direct correlation between $\Gamma(T)$ and $\bar{H}_{hf}(T)$ does not exist particularly for $T \lesssim 200$ K where $\Gamma(T)$ is roughly constant while $\bar{H}_{hf}(T)$ continues to increase as the temperature is lowered below 200 K. In view of our observation that *local* —spin-density fluctuations make a sizable contribution to thermal demagnetization over a wide range of temperatures including those in the close proximity to T_C, the above comparison between $\Gamma(T)$ and $\bar{H}_{hf}(T)$ points to the inherent limitation of the TP and Window methods in that none of them incorporates the relaxation contribution to Γ and $\bar{H}_{hf}(T)$ (this contribution is reflected more directly in Γ than in $\bar{H}_{hf}$), as already mentioned in Sec. III B 2.

5. Intensity ratio and the magnetic moment alignment

The temperature dependence of the *average* intensity ratios b^W, b^{FM}, and b^{cl} shown in Fig. 6(d) demonstrates that $b^W(T)$ conforms very well with $b^{FM}(T)$ in that both of them exhibit a sharp fall for $T \lesssim 1.5T_f$, a very weak or even no variation (within error limits) with temperature in the intermediate range 50 K $\lesssim T \lesssim$ 200 K and a steep rise for $T >$ 200 K as contrasted with a roughly constant value of $b^{cl} = 1.55(10)$ for $T \lesssim 150$ K, and a rapid increase in $b^{cl}(T)$ for $T >$ 150 K. These features of the $b^W(T)$ or $b^{FM}(T)$ and $b^{cl}(T)$ data have the following physical implications. The intensity ratio b, by virtue of its definition

$$b = 4\sin^2\theta/(1+\cos^2\theta) , \tag{22}$$

in terms of the angle θ between the γ-ray and *local* magnetic hyperfine-field (or *local* magnetic moment) directions, provides useful information about the local-spin arrangement. According to Eq. (22), for a perfectly random alignment of the local moments (spin-glass order), $b = 2.0$ whereas b assumes the limiting values 0 and 4 when all the moments are alighted *parallel* ($\theta = 0°$) and *perpendicular* ($\theta = 90°$) to the γ-ray direction, respectively. The average intensity ratio b therefore reflects the *average* orientation of the moments. Equation (22), when rewritten in the form

$$\langle \cos^2\theta \rangle = (4-b)/(4+b) \text{ or } \langle \sin^2\theta \rangle = 2b/(4+b) , \tag{23}$$

demonstrates that the mean angle $\langle \theta^{FM} \rangle$ corresponding to b^{FM} (or b^W) increases from 59° to 61° as b^{FM} decreases from 2.5 to 2.3 in the temperature range 50 K $\lesssim T \lesssim$ 200 K. In Eq. (23), $\langle\ \rangle$ denotes the average over the distribution of angle θ. The calculated values of $\langle \theta^{FM} \rangle$ indicate that, on average, the moments point 30° out of the sample plane presumably due to the competition between the magnetic anisotropy and demagnetization fields; the former anisotropy field tends to orient the moments away from the sample plane while the latter one tends to constrain them to the sample plane. A rapid decline in the value of b^{FM} or b^W for $T \lesssim 1.5T_f$ is, therefore, a manifestation of a steep increase in the strength of the *local* random anisotropy (LRA) fields,[5] which develop at the interface between the frozen FM clusters and the FM matrix, as the temperature is lowered below T_f and the freezing process progressively curtails the freedom of the spin

clusters around their random *mean* orientations. These LRA fields may, in turn, be responsible for a slight canting of the spins within the FM matrix and thereby result in the softening of the spin-wave modes. Note that the finding that $b^{\mathrm{FM}} \rightarrow 2$ at $T = 5$ K should *not* be interpreted as a transition to a *pure* (cluster) spin-glass state or alternatively, termed as a complete destruction of the long-range ferromagnetic order due to the imposition of a large LRA field on the FM matrix by the clusters frozen in random orientations, for the following reasons. (i) Spontaneous magnetization does not go to zero[5] as $T \rightarrow 5$ K (Fig. 3). (ii) At 5 K, b^{cl} has a value which is quite different from 2.0. (iii) Values of b close to 2.0 have also been previously reported[58,59] at temperatures as low as 4.2 K for Fe-rich amorphous $Fe_{100-x}B_x$ alloys, which do not exhibit a reentrant behavior at low temperatures. Existence of a mixed state for $T < T_f$ is also corroborated by the persistence of a well-defined domain structure down to[26,27] 4.2 K in a-$Fe_{90+x}Zr_{10-x}$ alloys.

In sharp contrast with the decrease in b^{FM} as the temperature is lowered through T_f ($=40$ K), b^{cl} stays constant at a value of 1.55(10) from $T \simeq 150$ K down to the lowest temperature. This value of b^{cl}, when substituted in Eq. (23), yields the result $\langle \theta^{\mathrm{cl}} \rangle = 48(2)°$. While $\langle \theta^{\mathrm{cl}} \rangle \cong 45°$ implies that the "out-of-plane" magnetic anisotropy energy and the demagnetization energy are nearly of the same magnitude for the spin clusters, the temperature-independent nature of b^{cl} for $T \lesssim 150$ K suggests that the freezing of spin clusters in *nearly* random orientations starts at a temperature well above T_f but $\lesssim 150$ K. Our $\chi_{\mathrm{hf}}(T)$ data (Sec. III A) and the *absence* of a slope change at $T = T_f$ in the temperature dependence of the SANS intensity[29] and spontaneous resistivity anisotropy[33] are consistent with this inference. A sudden increase in $b^{\mathrm{cl}}(T)$ for $T > 150$ K as well as in $b^{\mathrm{FM}}(T)$ for $T > 200$ K towards $b = 4.0$ reflects the dominance of the demagnetization effects as a result of a drastic reduction in the magnetic anisotropy for temperatures close to T_C.

IV. SUMMARY AND CONCLUSIONS

The results of a detailed magnetization and Mössbauer study of the amorphous $Fe_{90}Zr_{10}$ alloy are presented and discussed in the light of the existing theories. The main conclusions that can be drawn from a critical analysis of the data are as follows.

(i) The dominant contribution to the thermal demagnetization of spontaneous magnetization in different temperature ranges arises from spin-wave excitations for $T \lesssim 0.25T_c$, single-particle excitations and *local*—spin-density fluctuations for $0.38T_C \lesssim T \lesssim 0.88T_C$, and enhanced fluctuations in the *local* magnetization for $0.89T_C \lesssim T \lesssim 0.98T_C$.

(ii) The external magnetic fields of strength $\gtrsim 5$ kOe suppress the *local*—spin-density fluctuations completely and hence the temperature dependence of the "in-field" magnetization is solely governed by the spin-wave and single-particle excitations for temperatures up to $0.95T_C$.

(iii) The spin-wave stiffness coefficient is *independent* of the external magnetic field in the range $5\ \mathrm{kOe} \leq H \leq 15$ kOe.

(iv) The softening of the spin-wave modes takes place for $T \lesssim 60$ K ($\simeq 1.5T_f$).

(v) Contrary to the claim recently made by Ryan and Ren,[16] the magnetic hyperfine-field distribution is *bimodal* in the sense that the low-field component appears as a shoulder on the low-field side of the main peak.

(vi) The spin freezing does not begin at T_f but at a temperature $\simeq 3T_f$ and the freezing process proceeds gradually over a wide temperature range from about 130 K down to 4.2 K.

(vii) The above observations (v) and (vi) are *not* consistent with the predictions of the transverse spin freezing model.

(viii) In consonance with the results of earlier bulk magnetization and ferromagnetic resonance[22–25] measurements on a-$Fe_{90}Zr_{10}$, the low-field spin (LFS) fraction increases at the expense of the high-field spin (HFS) fraction as the temperature is increased beyond $T \simeq 150$ K so much so that the LFS fraction amounts to about 90% of the total Fe spins at $T \simeq T_C$.

(ix) The observation that the spontaneous magnetization does not go to zero at any temperature below the "freezing" temperature T_f provides conclusive evidence for the existence of a "mixed" phase (ferromagnetic order coexists with cluster spin-glass order) for $T < T_f$.

(x) Great caution has to be exercised while comparing the moment values computed from $\bar{H}_{\mathrm{hf}}$ using the conversion factor of 150 kOe/μ_B, valid for α-Fe, with those directly measured. The customary practice of attributing the low-field peak in $P(H_{\mathrm{hf}})$ to the presence of γ-Fe regions in the amorphous FM matrix is *incorrect.*

(xi) The methods employed hitherto to analyze the Mössbauer spectra recorded on the a-$Fe_{90+x}Zr_{10-x}$ alloys do not take into account the relaxation contribution which arises from the *local*—spin-density fluctuations (and hence from hyperfine-field fluctuations) and is dominant over a wide range of intermediate temperatures in these noncrystalline materials. A theory which incorporates the effects of the fluctuations in the hyperfine field as well as of a distribution of hyperfine fields (caused by the structural fluctuations in amorphous spin systems) on the Mössbauer line shape is called for.

(xii) The *finite* FM spin clusters plus *infinite* FM matrix model but not the *finite*—AFM-spin-clusters–FM-matrix picture provides a satisfactory explanation for all the diverse aspects of magnetization and Mössbauer results.

Note added in proof. After the submission of this manuscript the authors came across a paper by Ren and Ryan[60] in which they have independently arrived at the result that the relaxation contribution to the ME spectra is important in amorphous Fe-rich Fe-Zr alloys.

ACKNOWLEDGMENTS

This work was supported by the Department of Science and Technology, New Delhi, under Grant No. SP/S2/M21/86. The authors are thankful to Dr. G. Rajaram for rendering assistance during the initial stages of Mössbauer measurements. One of us (V.S.) is grateful to the Council of Scientific and Industrial Research, New Delhi, for partial support.

[1]H. Hiroyoshi and K. Fukamichi, J. Appl. Phys. **53**, 2226 (1982).
[2]S. N. Kaul, Phys. Rev. B **27**, 6923 (1983).
[3]W. Beck and H. Kronmüller, Phys. Status Solidi B **132**, 449 (1985).
[4]S. N. Kaul, J. Phys. F **18**, 2089 (1988).
[5]S. N. Kaul, J. Phys.: Condens. Matter **3**, 4027 (1991).
[6]M. Ghafari, U. Gonser, H.-G. Wagner, and M. Naka, Nucl. Instrum. Methods **199**, 197 (1982).
[7]H. Yamamoto, H. Onodera, K. Hosoyama, T. Masumoto, and H. Yamauchi, J. Magn. Magn. Mater. **31-34**, 1579 (1983).
[8]P. Deppe, K. Fukamichi, F. S. Li, M. Rosenberg, and M. Sostarich, IEEE Trans. Magn. **MAG-20**, 1367 (1984).
[9]D. H. Ryan, J. M. D. Coey, E. Batalla, Z. Altounian, and J. O. Ström-Olsen, Phys. Rev. B **35**, 8630 (1987).
[10]D. H. Ryan, in *Magnetic Properites of Amorphous Metals,* edited by A. Hernando, V. Madurga, M. C. Sanchez-Trujillo, and M. Vazquez (Elsevier, Amsterdam, 1987), p. 244.
[11]S. N. Kaul, C. Bansal, T. Kumaran, and M. Havalgi, Phys. Rev. B **38**, 9248 (1988).
[12]D. H. Ryan, J. O. Ström-Olsen, R. Provencher, and M. Townsend, J. Appl. Phys. **64**, 5787 (1988).
[13]M. Ghafari, W. Keune, R. A. Brand, R. K. Day, and J. B. Dunlop, Mater. Sci. Eng. **99**, 65 (1988); M. Ghafari, N. Chmielek, W. Keune, and C. P. Foley, Physica B **161**, 222 (1989).
[14]D. A. Read, T. Moyo, S. Jassim, R. A. Dunlap, and G. C. Hallam, J. Magn. Magn. Mater. **82**, 87 (1989).
[15]V. Siruguri, S. N. Kaul, G. Rajaram, and G. Chandra, Proc. Solid State Phys. Sympos. (India) **31C**, 233 (1988), An. Fis. Ser. B **86**, 181 (1990).
[16]D. H. Ryan and H. Ren, J. Appl. Phys. **69**, 5057 (1991).
[17]S. N. Kaul, A. Hofmann, and H. Kronmüller, J. Phys. F **16**, 365 (1986).
[18]N. Saito, H. Hiroyoshi, K. Fukamichi, and Y. Nakagawa, J. Phys. F **16**, 911 (1986).
[19]S. N. Kaul, J. Appl. Phys. **61**, 451 (1987).
[20]D. A. Read, G. C. Hallam, and M. Chirwa, J. Magn. Magn. Mater. **82**, 83 (1989).
[21]H. Ma, H. P. Kunkel, and G. Williams, J. Phys.: Condens. Matter **3**, 5563 (1991).
[22]S. N. Kaul and V. Siruguri, An. Fis. Ser. B **86**, 70 (1990).
[23]S. N. Kaul and Ch. V. Mohan, J. Phys.: Condens. Matter **3**, 2703 (1991).
[24]S. N. Kaul and V. Siruguri, J. Phys.: Condens. Matter **4**, 505 (1992).
[25]S. N. Kaul and P. D. Babu, Phys. Rev. B **45**, 295 (1992).
[26]H. Lerchner and M. Rosenberg, Hyperfine Interact. **39**, 51 (1988).
[27]S. Senoussi, S. Hadjoudj, P. Jouret, J. Bilotte, and R. Fourmeaux, J. Appl. Phys. **63**, 4086 (1988).
[28]S. Hadjoudj, S. Senoussi, and D. H. Ryan, J. Appl. Phys. **67**, 5958 (1990).
[29]J. J. Rhyne, R. W. Erwin, J. A. Fernandez-Baca, and G. E. Fish, J. Appl. Phys. **63**, 4080 (1988); J. J. Rhyne and G. E. Fish, *ibid.* **57**, 3407 (1985).
[30]P. Pureur, W. H. Schreiner, J. V. Kunzler, D. H. Ryan, and J. M. D. Coey, Solid State Commun. **65**, 163 (1988), and references quoted therein.
[31]Ch. V. Mohan, P. D. Babu, M. Sambasiva Rao, T. Lucinski, and S. N. Kaul (unpublished).
[32]S. N. Kaul, P. D. Babu, and Ch. V. Mohan (unpublished).
[33]H. Ma, Z. Wang, H. P. Kunkel, G. Williams, and D. H. Ryan, J. Appl. Phys. **67**, 5964 (1990).
[34]W. H. Kettler, R. Wernhardt, and M. Rosenberg, Rev. Sci. Instrum. **57**, 3053 (1986).
[35]M. Gabay and G. Toulouse, Phys. Rev. Lett. **47**, 201 (1981).
[36]S. N. Kaul, IEEE Trans. Magn. **MAG-20**, 1290 (1984); J. Magn. Magn. Mater **53**, 5 (1985).
[37]J. A. Heller, E. F. Wassermann, M. F. Braun, and R. A. Brand, J. Magn. Magn. Mater. **54-57**, 307 (1986).
[38]D. A. Read, T. Moyo, and G. C. Hallam, J. Magn. Magn. Mater. **54-57**, 309 (1986).
[39]D. A. Read, T. Moyo, and G. C. Hallam, J. Magn. Magn. Mater. **44**, 279 (1984).
[40]J. Takeuchi and Y. Masuda, J. Phys. Soc. Jpn. **46**, 468 (1979).
[41]S. N. Kaul, Solid State Commun. **52**, 1015 (1984).
[42]F. Keffer, in *Encyclopedia of Physics,* edited by H. P. J. Wign (Springer, Berlin, 1966), Vol. XVIII, Pt. 2, p. 1.
[43]J. Mathon and E. P. Wohlfarth, Proc. R. Soc. London, Ser. A **302**, 409 (1968).
[44]S. N. Kaul and P. D. Babu, J. Phys.: Condens. Matter (to be published).
[45]S. G. Mishra, Mod. Phys. Lett. B **4**, 83 (1990).
[46]G. G. Lonzarich and L. Taillefer, J. Phys. C **18**, 4339 (1985).
[47]C. L. Chien and H. S. Chen, J. Phys. (Paris) Colloq. **40**, C2-118 (1979).
[48]B. Window, J. Phys. E **4**, 401 (1971).
[49]H. Keller, J. App. Phys. **52**, 5268 (1981).
[50]A. H. Morrish, R. J. Pollard, Z. S. Wronski, and A. Calka, Phys. Rev. B **32**, 7528 (1985).
[51]M. Blume and J. A. Tjon, Phys. Rev. **165**, 446 (1968).
[52]D. G. Rancourt, S. R. Julian, and J. M. Daniels, J. Magn. Magn. Mater. **51**, 83 (1985); R. G. Rancourt, H. H. A. Smit, and R. C. Theil, *ibid.* **66**, 121 (1987).
[53]V. Jaccarino, L. R. Walker, and G. K. Wertheim, Phys. Rev. Lett. **13**, 752 (1964).
[54]H. Callen, D. Hone, and A. Heeger, Phys. Lett. **17**, 233 (1965).
[55]T. Wolfram and W. Hall, Phys. Rev. **143**, 284 (1966).
[56]P. Panissod, J. Durand, and J. I. Budnick, Nucl. Instrum. Methods **199**, 99 (1982).
[57]J. Balogh and I. Vincze, Solid State Commun. **25**, 695 (1978).
[58]R. A. Dunlap and G. Stroink, J. Phys. F **14**, 3083 (1984).
[59]S. J. Harker and R. J. Pollard, J. Phys.: Condens. Matter **1**, 8269 (1989).
[60]H. Ren and D. H. Ryan, J. Appl. Phys. **70**, 5837 (1991).